Iranian Journal of Medical Physics

ijmp.mums.ac.ir

Efficiency Comparison between Radiotherapy Alone And In The Presence of Radio- or Photo- Sensitizers on Viability of DFW and HT29 Cell Lines: From Simulations to Experimental Results

Farideh. S. Hosseini[1], Nadia Naghavi[1*], Ameneh Sazgarnia[2,3], Atefeh Vejdani Noghreiyan[3,4]

1. Department of Electrical Engineering, Ferdowsi University of Mashhad, Mashhad, Iran.
2. Medical Physics Research Center, Mashhad University of Medical Sciences, Mashhad, Iran.
3. Department of Medical Physics, Faculty of Medicine, University of Medical Sciences, Mashhad, Iran
4. Department of Medical Physics Radiobiology and Radiation Protection, School of Medicine, Babol University of Medical Sciences, Babol, Iran

ARTICLE INFO

Article type:
Original Paper

Article history:
Received: Jan 18, 2024
Accepted: Jun 08, 2024

Keywords:
Radiation-Sensitizing Agents
Singlet Oxygen
Nanocomposites
Mathematical Modeling
Combined Modality Therapy

ABSTRACT

Introduction: Radiotherapy (RT) is a conventional cancer treatment which address needs of most cancerous patients. However, toxicity of high X-ray energies increases side effects to the normal tissues. Combining RT with agents like radiosensitizers and photosensitizers has improved its effectiveness. This study presents a mathematical model of X-ray induced photodynamic therapy (XPDT) and validates its results with relevant experimental data.

Material and Methods: This study developed XPDT using TiO_2 nanoparticles as nanoscintillators and PpIX as a photosensitizer. A multi-scale physicochemical model was created to simulate XPDT, highlighting the role of molecular oxygen in its efficiency. XPDT outcomes were compared with RT—both alone and combined with radiosensitizers—using data from two radioresistant cell lines: DFW and HT-29.

Results: Simulations and experimental data showed XPDT to be more effective than RT alone or RT with TiO_2. Simulations estimated XPDT reduced cell viability by 45.28% in DFW and 59.02% in HT-29 compared to RT. Modeling helped estimate both apoptotic and necrotic cell death, and a minimum XPDT efficiency was defined based on cells affected synchronously by both RT and PDT. At 4 Gy irradiation and 4 mg/ml nanocomplex concentration, at least 13.22% of DFW and 21.23% of HT-29 cells were eliminated. TiO_2-enhanced RT had the most effects in cell killing during XPDT.

Conclusion: XPDT showed higher efficacy in targeting cancer cells compared to RT or PDT alone. However, further research is needed to understand certain unexpected cellular responses under specific treatment conditions.

► *Please cite this article as:*
Hosseini FS, Naghavi N, Sazgarnia A, Vejdani Noghreiyan A. Efficiency Comparison between Radiotherapy Alone And In The Presence of Radio- or Photo- Sensitizers on Viability of DFW and HT29 Cell Lines: From Simulations to Experimental Results.. Iran J Med Phys 2025; 22: 77-88. 10.22038/ijmp.2024.77566.2366.

Introduction

Excellent tissue penetration depth of ionizing radiation has converted radiotherapy (RT) as one of the most effective methods for malignant tumor treatments. However, toxicity of radiation on surrounding healthy tissues increases with increasing radiation doses. So, the most important goal of RT is to destroy tumor cells while reducing side effects. There are various factors that affect efficiency of RT such as presence of radio-sensitizer or radio-resistant agents (1-3). Radio-sensitizers are agents that enhance the effects of RT. Among different types, metallic nanoparticles causing localized damage to DNA and other targeted organelles of cancer cells by selectively scattering and/or absorbing X-rays. Thus, they can decrease total radiation dose to the tissues and then minimize side effects of ionizing radiation (4).

Photodynamic therapy (PDT), on the other hand, is a low toxicity, less invasive and highly selective therapeutic modality for malignant and not malignant lesions (5, 6). During this method, light with a specific wavelength absorbed by a drug called photosensitizer (PS) to produce some reactive oxygen species (ROSs) in the presence of molecular oxygen. ROSs are cytotoxic for the cells, so PDT can work as well as surgery or radiotherapy in treating certain kinds of cancers (7). However, PDT is mostly used to superficial disease or surface tumors, because of high tissue absorption and scattering of visible light in the normal tissues (8).

X-ray induced photodynamic therapy (XPDT) is a new modality of cancer treatment that benefits from RT and PDT, simultaneously. In addition to ionizing toxicity of X-rays, they can penetrate in deep seated

*Corresponding Author: Email: nn.naghavi@gmail.com

tumors and initiate photodynamic reactions that can directly target cancer cells (8). In other words, XPDT cause cell damage through the two different mechanisms of radiation energy transfer and photodynamic activation. As a result, XPDT interplay to attack both cell membrane and DNA, leading to lethal damage that is beyond the repairs of the cells (9). Moreover, XPDT uses much lower radiation dose than that of traditional clinical RT (10).

Along with the advancement of nanotechnology, Chen and Zhang (11) proposed the first concept of nanoparticle-mediated XPDT in 2006. The principle of XPDT is to use a physical transducer called nanoscintillator (NSc) to transfer X-rays to optical luminescence and activate conjugated PSs. At the same time, the absorbed ionizing radiation can generate cytotoxic species and damage DNA of tumor cells. Cellular experiments have demonstrated that XPDT is not only a PDT derivative, but also a type of RT derivative (9, 10). In addition, synergy effects of the two RT and PDT components lead to increased mortality rate compared to the sum of each component mortality rate alone (12).

Morgan et al. in 2009 made the first calculations of physical parameters required for efficient XPDT (13). The study combined results of before literature based on this assumption that X-ray photons which hit a NSc would transfer all of their energy to it while Monte Carlo simulations of Bulin et al. in 2015 reported that only a few percentage of X-ray energy will transfer to light within the scintillator and the other part of energy transferred to the surrounding tissues (14). Following this results, Klein et al. in 2019 proposed a simple model to compute the luminescence yield of nanoparticles in tissues (15). Although this electron cross section model provides an upper bound for the actual number of scintillation photons, it is not able to completely predict XPDT efficacy reported during pre-clinical tests (10). Experimental studies have shown that XPDT is actually a PDT and RT combination and not just a PDT derivative [7].

Although, several studies have been conducted in XPDT modeling, none of them have paid attention to the simultaneous presence and contribution of the two main components of PDT and RT and their synergistic effects. Also, there has been little focus on the key role of molecular oxygen and tissue oxygenation parameters in treatment efficiency.

In this paper, we have attempted to estimate the contribution of RT and PDT components as well as their synergy effects to predict the apoptotic and necrotic cellular death during XPDT. Then, we compared our simulation results with the results of radiotherapy and radiotherapy in the presence of radiosensitizers. In this regards, we used our newly developed physicochemical model of XPDT to simulate molecular oxygen as one of the important factors determining the amount of produced $^1O_2$ and also XPDT efficiency (12, 16). Results of the model, then have evaluated with appropriate cell viability data of DFW and HT29 cell lines with MTT assay. HT29 and DFW are known to be less sensitive (17) and resistant (18) cell lines to RT, respectively and were chosen to check whether XPDT affects them or not.

Materials and Methods

Mathematical Model

In order to predict XPDT efficiency on DFW and HT29 cell lines, we firstly model tumor cell growth in order to estimate surrounding oxygen concentration at the time of treatment. Then according to this concentration, we estimate the efficiency of PDT component as well as RT component of XPDT. There are various mathematical models describing different parts of tumor growth and invasion (19-25), but we simply focus on the interactions of tumor cells with the important microenvironmental molecules. So, modeling process includes three coupled models named as nutrient diffusion, cell growth and treatment.

Nutrient Diffusion

At this part, we consider three different molecules of i includes oxygen (O_2), glucose (G), and microenvironmental pH via production of protons (H), diffuse across the point (x,y), with diffusion constant D_i. The concentration $C_i(x,y)$ is estimated as (26):

$$\frac{\partial C_i(x,y)}{\partial t} = D_i \nabla^2 C_i(x,y) + W_i(x,y) \quad (1)$$

Where W_i is the production or consumption rate of the molecule i.

Cell Growth

We model three cellular processes of cell cycling, mitosis and cellular death in this section. Moreover, each tumor cell may be at one of the proliferating, quiescent, dead or treated states at each time step. This cell states determined by three factors of microenvironmental pH, the amount of ATP produced by each cell and availability of empty space around. We use some cellular automaton rules to update the status of each cell in each time step (Figure 1). We initially assume that all of tumor cells are proliferative and progress in the cell cycle stages (G_1, S, G_2, M) with consuming nutrients (O_2 and G) and produce metabolic waste (H). When they reach to the mitosis stage, if there is an empty space around a mitotic cell, it divides in two daughter cells, one stay in the space of mother cell and the other goes randomly to one of the surrounding empty spaces and the cell cycle repeats again. In addition, if the cell does not satisfy the threshold conditions of A_q, A_d and A_{res} its state changes from proliferative to quiescent, necrotic or apoptotic, respectively (Figure 1).

A treated cell includes one of the necrotic or apoptotic cell formed at the time of the treatment, depending on destroying by PDT or RT component of XPDT.

We assume that oxygen consumption rate of W_{O2} is proportional to oxygen concentration $C_{O2}(x,y)$ and obeys Michaelis–Menten kinetics as [25]:

$$W_{O2}(x,y) = -V_{O2}\frac{C_{O2}(x,y)}{C_{O2}(x,y)+K_{O2}} \quad (2)$$

Where V_{O2} is the maximum oxygen consumption and K_{O2} is the half maximum oxygen concentration. As well, glucose consumption rate is proportional to the need of meet normal ATP demand by the cells and estimated by a Michaelis–Menten term as [24]:

$$W_G(x,y) = -\left(\frac{P_G A_0}{2} + \frac{27W_{O2}(x,y)}{10}\right)\frac{C_G(x,y)}{C_G(x,y)+K_G} \quad (3)$$

Where $A_0 = \frac{29}{5}V_{O2}$ is the baseline production rate of ATP, and $C_G(x,y)$ and K_G are defined as glucose concentration, and half maximum concentration, respectively.

It has been shown that tumors altered glucose metabolism during the process called Warburg effect. The coefficient P_G at equation (3), is representing the Warburg effect that $P_G = 1$ denotes normal glucose consumption of cancer cells and $P_G > 1$, corresponds to that tumor cells will consume more glucose than needed. So, by defining $\frac{W_A}{A_0}$, as the the target ATP production rate, ATP consumption rate $W_A(x,y)$ and hydrogen consumption rate $W_H(x,y)$ are estimated as [24]:

$$W_A(x,y) = -\left(2W_G(x,y) + \frac{27W_{O2}(x,y)}{5}\right) \quad (4)$$

And

$$W_H(x,y) = K_H\left(\frac{29(P_G V_{O2}(x,y) + W_{O2}(x,y))}{5}\right) \quad (5)$$

Where parameter K_H accounts for proton buffering in the tumor microenvironment.

Treatment Model

During XPDT reactions, when PS is irradiated in the ground state, it absorbs light produced by NSc and reaches the singlet excited state *S1* (Figure 2). It can then lose its energy by fluorescence emission and return to the ground state or transfer to the longer-lived triplet state *T1*. At this stage, depending on the type of PS and the relative concentrations of substrate and oxygen, two types of PDT reactions can occur [5,6]. In type I reactions, *T1* transfers a proton or an electron directly to a substrate, such as a cell membrane or an isolated molecule, to form radical anions or cations, respectively. These radicals may react with oxygen to produce ROS. In type II reactions, *T1* can transfer its energy directly to ground-state molecular oxygen to form singlet oxygen ($^1O_2$, also known as ROS) [26]. It is assumed that singlet oxygen is the main cytotoxic agent for most reported PSs and that the efficacy of PDT is directly related to the efficiency of $^1O_2$ production [27].

In modeling XPDT, we consider the contribution of RT and PDT components separately as well as synergy effects of them in killing cancer cells. To estimate the response of cancer cells to RT, we use Linear Quadratic LQ) model. According to this model, the proportion of cells surviving an irradiation of dose *D* (Gray) is [29]:

$$SF(D) = \exp(-\alpha D - \beta D^2) \quad (6)$$

Where α (Gy^{-1}) and β (Gy^{-2}) are cell-specific radiosensitivity parameters that are related to the probabilities of double-strand breaks in DNA and their repair, respectively (27). On the other hand, radiosensitizers have different mechanisms on effective killing cancer cells, and we assume all radiosensitization processes together as a linear excitation of the form *S(C)=(1+bC)* with a net excitation effect. The radiation-induced mass transfer is given by [29] to make the model generally applicable as:

$$SF(C,D) = \exp[-(1+bC)(\alpha D + \beta D^2)] \quad (7)$$

Where b is a pharmacodynamic parameter associated with the radiosensitizing effects and C is plasma concentration of the radiosensitizer. We called the model of RT in the presence of radiosensitizers as RT+RS model.

To model the PDT component of XPDT, we focus on the production of $^1O_2$ as the dominant molecule in type II PDT reactions. Since the dynamic processes of PDT are very fast (~μs or less), the macroscopic model of $^1O_2$ production on a time scale of seconds to hours can be written as [30]:

$$[^1O_2] = S_\Delta\, \emptyset_t k_0\, \tau_\Delta [S_0]\left(\frac{C_{O2}(x,y)}{C_{O2}(x,y)+ Kp/Kot}\right) \quad (8)$$

Where S_Δ is the fraction of *T1-O₂* reaction, $\emptyset_t$ is PS triplet yield, k_0 is the photon absorption rate of PS per PS concentration, τ_Δ is $^1O_2$ life time, *[S₀]* is the concentration of PS in its ground state, Kp/Kot is called as the oxygen quenching threshold concentration and *$C_{O2}(x,y)$* is oxygen concentration at the point *(x,y)*.

According to the equation (8), the produced $^1O_2$ concentration during PDT depends on PS parameters defining energy transfer in PS and a term describes oxygen concentration. By substituting the corresponding XPDT energy transfer mechanism proposed by Klein et al. [13] and assuming that all photons are converted to $^1O_2$ molecules, we obtain:

$$[^1O_2] = N_{scint}\left[\frac{\text{photons}}{cm^3}\right] \times 1\left[\frac{1O2\ \text{molecules}}{\text{photons}}\right]\frac{C_{o2}(x,y)}{C_{o2}(x,y)+ Kp/Kot} \quad (9)$$

Where N_{scint} is density of scintillation photons emitted by a dilute suspension of NSc and depends on some physical parameters like radiation dosage *D*, nanoscintillator concentration C_{sc}, scintillator light yield Y_{sc} as (15):

$$N_{scint}\left[\frac{\text{photons}}{cm^3}\right] = D\left[\frac{J}{kg}\right] \times 10^{-3}\left[\frac{kg}{g}\right] \times 6.2 \times 10^{12}\left[\frac{MeV}{J}\right] \times C_{sc}\left[\frac{g}{cm^3}\right] \times \frac{(\mu/\rho)_{sc}[MeV \times cm^2 g^{-1}]}{(\mu/\rho)_{tissue}[MeV \times cm^2 g^{-1}]} \times Y_{sc}\left[\frac{\text{photons}}{MeV}\right] \quad (10)$$

where μ/ρ is the electron cross section for NSc tissue and materials, which can be obtained from the ESTAR database, maintained by the National Institute of Standards and Technology (NIST).

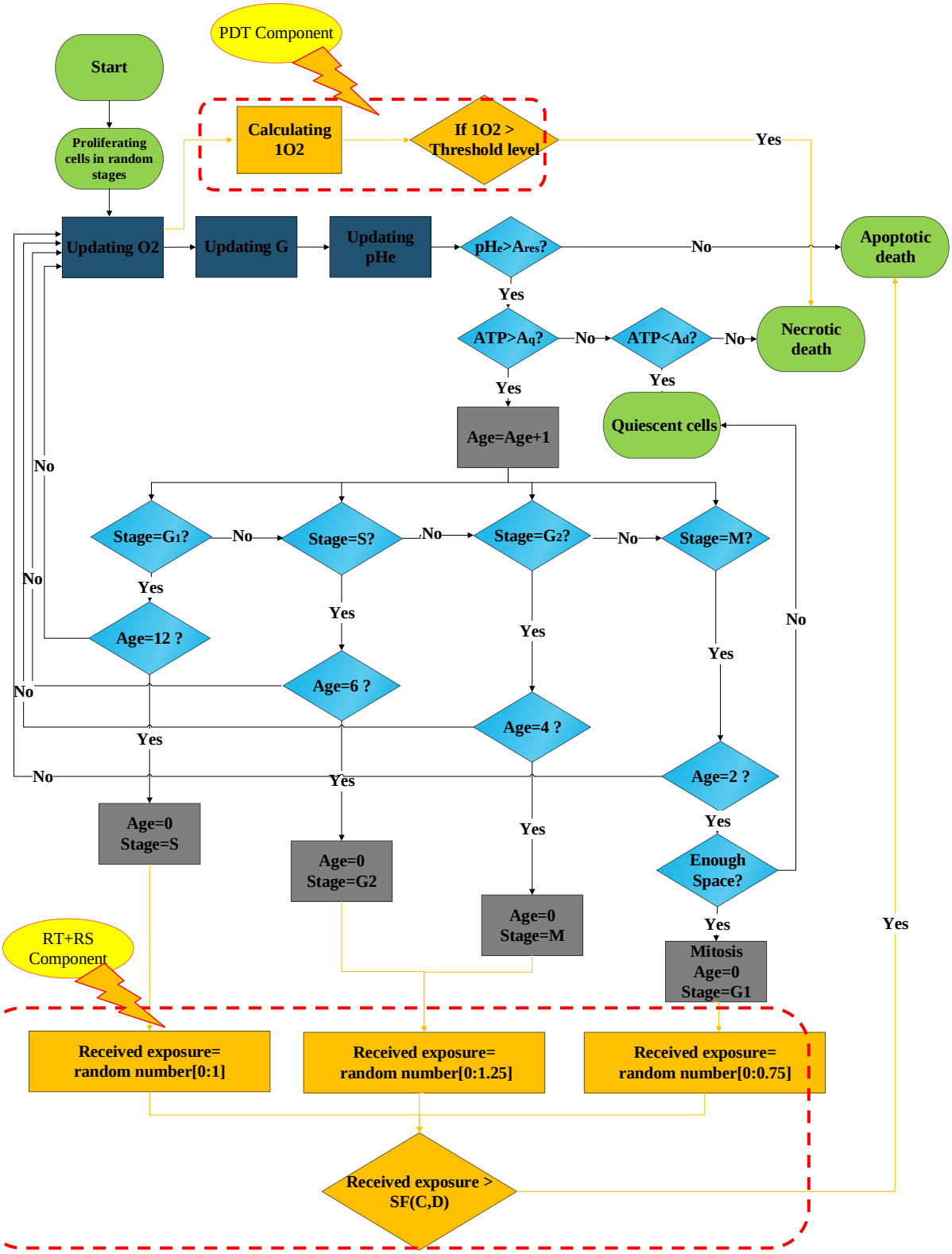

Figure 1. Model overview includes cellular automaton rules for coupling of nutrient diffusion, cell growth and treatment model. The dashed lines show how to apply RT and PDT components of XPDT at the treatment time.

Finally, the corresponding number of $^1O_2$ produced per cell (N_{1O2}) is calculated by multiplying the cell volume by [13]:

$$N_{1O2}\left[\frac{102\ \text{molecules}}{\text{cells}}\right] = C_{1O2}\left[\frac{102\ \text{molecules}}{cm^3}\right] \times V_{cell}\left[\frac{cm^3}{cell}\right] \quad (11)$$

Initial and boundary conditions: simulation of the model carried out on a grid of 200×200 point, which is a discretization of the unit square [0,1] × [0,1], with a space step of h= 0.005. Experimental tests done in 96-well plates that approximately equivalent to a tissue with dimensions of 5 mm × 5 mm, representing a grid size of Δx = Δy = 25 μm which corresponds to the size of a tumor cell (19). We assume an initially circular tumor with radius of 0.25 and 0.22 which equals to about 8000 and 6000 tumor cells for HT29 and DFW cell lines, respectively in accordance with laboratory conditions. Initial pH value of the tumor microenvironment is set to 7.4. An initial oxygen and glucose concentrations of 5.2×10^{-6} mol/L and 5×10^{-3} mol/L are set in the tumor microenvironment, respectively (28). No flux boundary conditions are adopted for the interstitial diffusion equations. The required parameter values are given in **Error! Not a valid bookmark self-reference.**.

Experimental Data

We used the recently developed nanocomposite Ti-MSN/PpIX (29) which includes TiO_2 self-lighting nanoparticles as NSc, PpIX as PS and mesoporous silica nanoparticles (MSN) as PS and NSc carrier. Under RT exposure, TiO_2 emits persistent luminescence that activates PpIX. The outcome is the generation of cytotoxic $^1O_2$, which causes cell death. More details about characterization of the synthesized nanocomposite referred to (29). The impact of XPDT on cells was investigated by MTT assay. DFW cell line, a depigmented melanoma subline obtained from DFB (another melanoma cell line) by limiting dilution and HT29, a human colon cancer cell line was provided by Pasteur Institute of Iran. Cells (8×10^3 cells/well HT29 and 6×10^3 cells/well DFW) were seeded in 96-well plates and incubated overnight. The cells then were grown in different groups of Ti-MSN/PpIX nanoparticles at concentration of 4 mg/ml. The control group with no additive and a group incubated with Ti-MSN were also considered. Ti-MSN nanoparticle concentrations were considered equal to the Ti-MSN/PpIX group (1, 2 and 4 mg/ml). After washing the cells with PBS, the plates were exposed to various doses of 6 MVp X-rays, separately includes 1, 2 and 4 Gy. After 48 hours, viability of the cells estimated by MTT assay so that 5 mg/ml of MTT solution was added and incubated for 4 hours at 37°C, then the supernatant was taken and 200 μl of DMSO was added to them to lyse the cells. Then viability of the cells was estimated as a percentage of the optical density (OD) of each sample relative to the untreated control group, which was set to 100% at a wavelength of 570 nm versus 630 nm. Further details on the experiments are referred to [32].

Table 1. Parameter values selected for mathematical modeling

Parameter	Description	Value	Unit	Reference
P_G	Up regulated glucose uptake rate	30	-	(28)
D_{O2}	Tissue oxygen diffusivity	$2.41*10^{-5}$	$mol.L^{-1}$	(30)
K_{O2}	Half-max O_2 concentration	$5*10^{-6}$	$mol.L^{-1}$	(31)
V_{O2}	Max O_2 consumption	$2.3*10^{-16}$	$mol.(cell.s)^{-1}$	(32)
D_G	Tissue glucose diffusivity	$9*10^{-5}$	$cm^2.s$-1	(33)
K_G	Half-max glucose concentration	$4*10^{-5}$	$mol.L^{-1}$	(31)
D_H	Tissue hydrogen ion diffusivity	$1.1*10^{-5}$	$cm^2.s^{-1}$	(33)
K_H	Proton buffering coefficient	$2.5*10^{-4}$	-	(26)
A_{res}	pH Cancer cell acid resistance	6	pH	(34)
A_d	ATP Threshold for death	0.3	-	(26)
A_q	ATP Threshold for quiescence	0.8	-	(26)
α_{DFW}	Probabilities of double-strand breaks in DNA of DFW cell line	0.002	Gy^{-1}	(35)
β_{DFW}	Probabilities of radiation repair of DFW cell line	0.01	Gy^{-2}	(35)
α_{HT29}	Probabilities of double-strand breaks in DNA of HT29 cell line	0.0928	Gy^{-1}	(36)
β_{HT29}	Probabilities of radiation repair of HT29 cell line	0.0203	Gy^{-2}	(36)
Y_{sc}	Light yield of scintillator	10^5	Photons/MeV	(15)
K_p/K_{ot}	oxygen quenching threshold concentration	$11.9*10^{-6}$	$mol.L^{-1}$	(37)

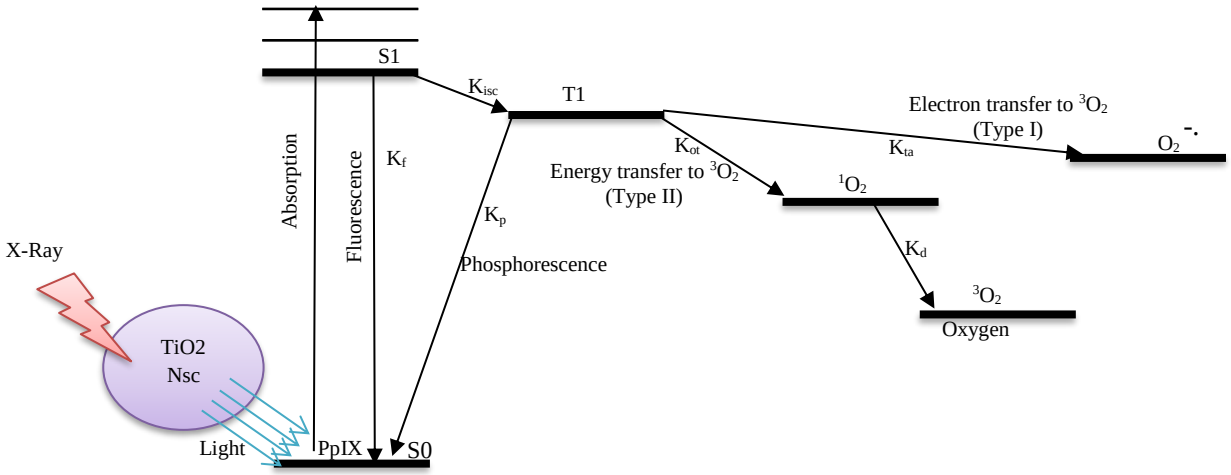

Figure 1. Activation of photosensitizer molecules (PpIX) during XPDT by the light transmitted by nanoscintillator (NSc) after X-ray excitation. Production of $^1O_2$ during type II of PDT reactions are as well as X-ray radiation are the two main components of XPDT for tumor cell killing(38).

Results

In order to estimate response of the model to RT in the presence and absence of radiosensitizers, we need reliable estimation of α and β radiosensitivity parameters for DFW and HT29 cell lines. In this regards, dose-viability curves were obtained for single doses (0– 4 Gy) and surviving fractions at those doses, were substituted into equation of the LQ model using curve fitting MATLAB calculation software. Then, α and β computed by carrying out the optimum convergence to approximate the survival curves. Figure 3 shows the fitted curves and parameter values. Based on the results, the negative small values of β obtained for the two cell lines so, the negative, large values for α/β. Regardless of the sign, it indicates that the tumor is very sensitive to the effects of fractionation. Although negative values of the α/β ratio are not realistic from a radiobiological point of view, it is not recommended to restrict negative values in radiobiological analyses because when the parameters are restricted, the overall estimates do not converge to the true value [42].

TiO_2 used in nanocomposite structure is a metallic nanoparticle with the effects of radiosensitization (39, 40) and nanoscintillation (11). Figure 4 shows the effects of concentration variations of NSc (also radiosensitizer) as well as nanocomposite (NP) in the presence and absence of X-rays (4 Gy where it needed) on the mean cell viability. According to the Figure 4(a), viability of both DFW and HT29 cell lines decreases as NSc concentration increases. Results estimated that monotherapy effects of NSc in the absence of any radiation dose decreased cell population to about 50% with increasing NSc concentration up to 4 mg/ml in both cell lines. However, the combination of NSc and X-ray well decreased cell viability in corresponding concentrations respect to monotherapy of NSc in both cell lines (except DFW in C=4 mg/ml).

Figure 4(b) compares NP toxicity with combination of NP and X-ray (XPDT) toxicity on the two cell lines. According to this figure, cell population significantly decreases with applying X-rays, specially in HT29 cell line. As well, in comparison with NSc toxicity (Figure 4(a)), NP had lower toxicity effects on both cell lines. So, using NSc in the structure of NP can reduce toxicity for the cells and is more compatible for the tissues.

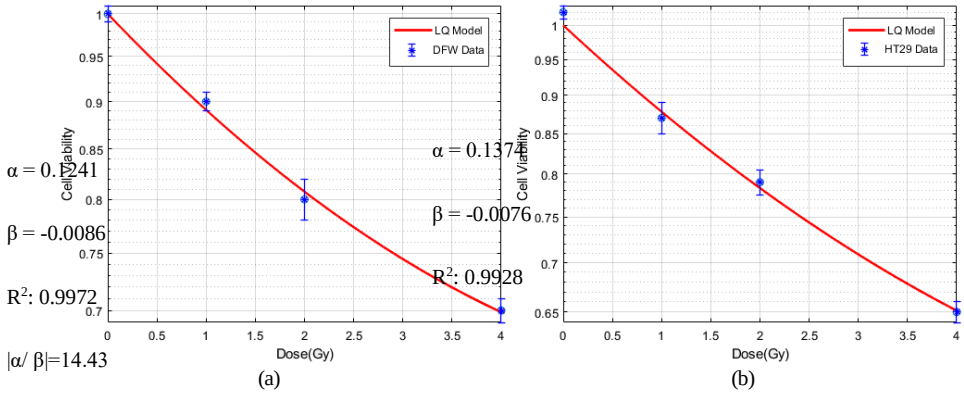

Figure 2. Cell viability of (a) DFW and (b) HT29 cell lines under X-ray radiationa ($6Mv_p$) and LQ parameter estimation for them.

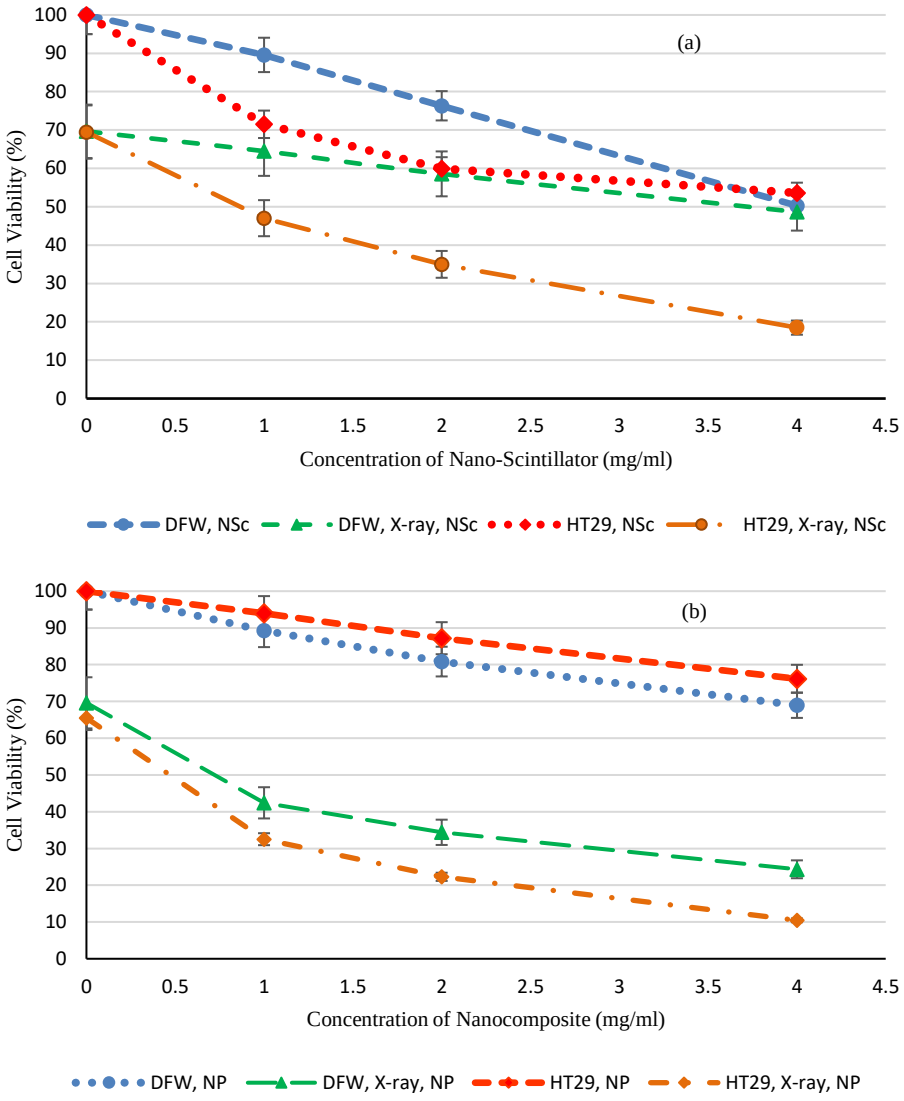

Figure 3.Simulation results of average cell viability ± standard deviation in different concentrations of (a) Nano-scintillator (NSc) and (b) Nanocomposite (NP) in the presence and absence of X-rays (4Gy) on DFW and HT29 cell lines.

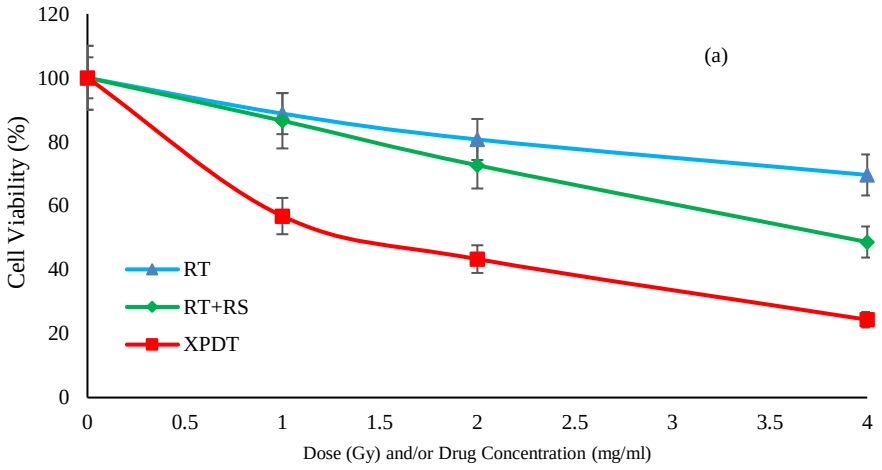

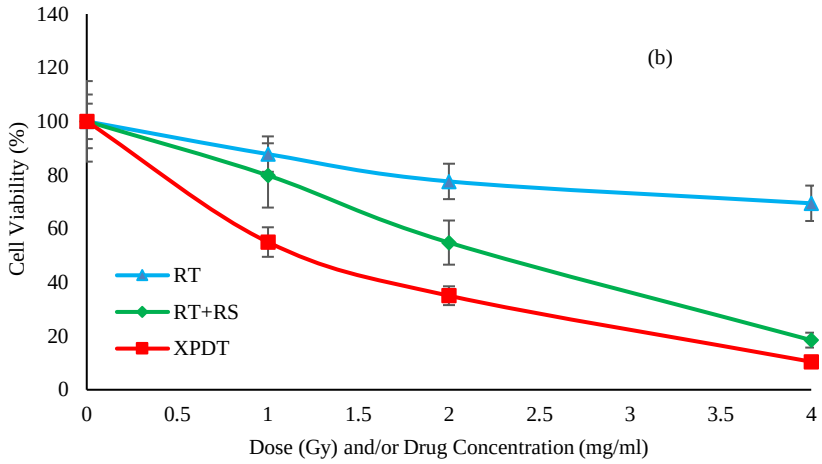

Figure 5. Comparison of mean cell viability ±standard deviation under the treatments of RT, RT+RS and XPDT for (a) DFW and (b) HT29 cell lines

Figure 5 shows the efficacy of radiotherapy (RT), RT in the presence of RS (RT+RS) and XPDT on the two cell lines of DFW and HT-29, separately. According to the results, RT alone (0-4 Gy) did not induce significant death while RT+RS and XPDT induced a large viability drops finally in dose of 4 Gy. As a comparison, at irradiation of 4 Gy and NP concentration of 4 mg/ml, cell viability reduced to 24.34% in DFW and 10.45% in HT29 cell lines while with RT only (4 Gy) cell viability reduced to 69.62% in DFW and 69.47% in HT29 cell lines. In corresponding conditions, NSc concentration of 4 mg/ml and radiation dose 4 Gy, RT+RS reduced cell viability to 48.64% in DFW and 18.49% in HT29 cell lines.

Figure 6 shows simulation results of tumor cells destroyed by different XPDT components in NP concentration of 4 mg/ml and radiation dose 4 Gy for DFW and HT29 cells, separately. It has been shown that PDT induces cell membrane damages and ionizing radiation cause DNA damages, so they synchronously induce tumor cell necrosis and apoptosis (10). With this assumption, we estimated apoptotic death during RT+RS component of XPDT in Figure 6 (a & d) and necrotic death during PDT component of XPDT in Figure 6 (b & e). Also, common cells targeted by both components of PDT and RT+RS, simultaneously (synergy effects) are shown in Figure 6 (c & f).

According to these figures, RT+RS (Apoptotic death) had the most effects on death rates of both cell lines during XPDT, so that 51.36% of cellular death in DFW and 81.51% in HT29 cell line is due to RT+RS. Also, common cells killed by the two components represent cells with the maximum probability death rates because they were targeted by both radiation and $^1O_2$ components and therefore, they predict the minimum efficiency of XPDT under specified conditions.

Comparison of model and experimental results of cell viability for DFW cells under 4 mg/ml of related drug concentration (where it needed) is shown in Figure 7. Regarding to the experimental results, XPDT had the most effects on cell death in all radiation doses (1, 2 and 4 Gy). However, in drug monotherapy group (0 Gy), XPDT showed lower effects on cell killing, respect to the RT+RS model. This indicates the toxicity of NSc reduces when it uses in the format of nanocomposite.

In-vitro results have also shown that production of light by scintillator (TiO_2), causing biological stimulation of cells and therefore increasing viability of them (29). On the other hand, presence of NSc inside the cells increasing possibility of photoelectric phenomenon. As a result, in some radiation doses of RT+RS model (2 and 4 Gy of RT+RS Data), biological stimulation dominates the photoelectric phenomenon, so cell viability increases unpredictably. While in radiation dose of 1 Gy (RT+RS Data), photoelectric phenomenon dominates the biological stimulation, therefore cell population decreases unexpected. This photoelectric phenomenon also occurred in XPDT-Data in this dose (Figure 7). These processes that have ignored in modelling, causing some differences between experimental results and related simulations.

In XPDT group, on the other hand, these problems have been reduced because the presence of an appropriate PS in the path of the light produced by scintillator absorbs it and balances the biological stimulation effects. However, in radiation dose of 4 Gy viability of cells increases out of expectation (XPDT Data) that may be due to the insufficient concentration of PS at the environment (41).

The results of RT, RT+RS and XPDT modeling and their comparison with the related experimental results of in-vitro HT29 cell line at corresponding drug concentration of 4 mg/ml (where it needed) are shown in Figure 8. Similar to the Figure 7, NP toxicity also was much lower than NSc toxicity on HT29 line. Also, XPDT showed significant differences (p-value< 0.032) compared to RT and RT+RS groups in all radiation doses. As in DFW cell line, production of light by scintillator in RT+RS group and therefore biological stimulation of HT29 cells gradually increases in D=2

and D=4. This effect is so large that causes a sudden increase in cell viability compared to dose 2 Gy. Presence of PS in XPDT groups and initiation of PDT reactions, reduces cell viability and balances this effect. However, insufficient concentration of PS in nanocomposite structure may be one of the reasons for unexpected increase in cell viability in dose 2 Gy (41).

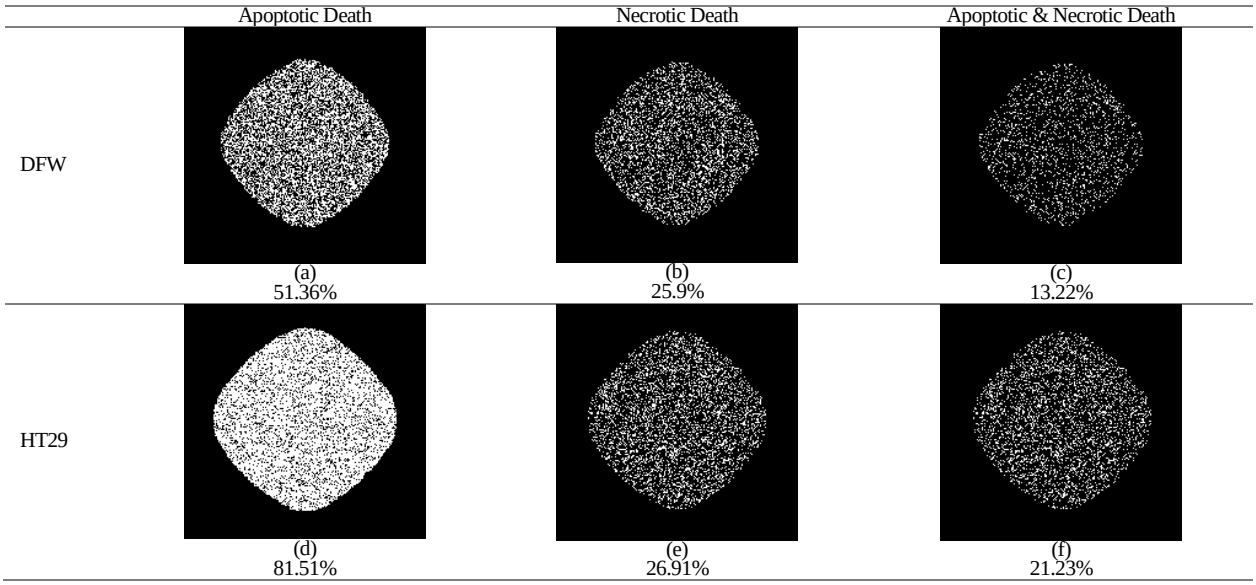

Figure 4. Model estimation of apoptotic and necrotic death for DFW and HT-29 cell lines during XPDT under 4 mg/ml nanocomposite concentration and radiation dose of 4 Gy.

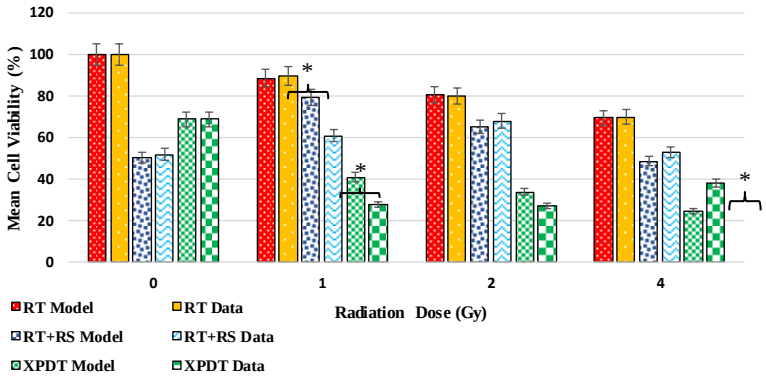

Figure 5. Comparison of RT, RT+RS and XPDT model results with the related experimental results in DFW cell line under dose variations of 0-4 Gy (* P-value<0.017).

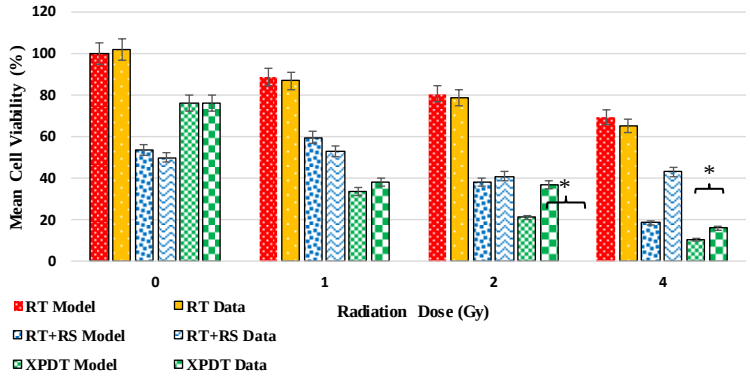

Figure 6. Comparison of RT, RT+RS and XPDT model results with the related experimental results in HT29 cell line under dose variations of 0-4 Gy (* P-value<0.023).

Discussion

In this study, a multi-scale physico-chemical model of XPDT was presented in order to model the contribution of XPDT components include PDT and RT. Then, we estimated XPDT efficiency mathematically and compared the results with RT only and RT in the presence of radiosensitizers (RT+RS). Simulation results validated with appropriate in-vitro results of RT, RT+RS and XPDT for DFW and HT29 cell lines. Each of the mentioned cell lines can represent a range of cancers. HT29 is one of the less sensitive types to RT (and even resistant to RT), which has been used as a representative of adenocarcinomas (17). DFW cell line, which is derived from melanoma, has known to be resistant to RT (18). This feature of the cells also observed by plotting dose-survival curves and parameter estimation of the LQ model.

Modeling the contribution of each components along with their synergistic effects made it possible to predict the minimum efficiency of XPDT at specific conditions. We introduced the number of cells targeted simultaneously by RT and PDT as the minimum efficiency of XPDT, because this multi objective targeting of the cells (both DNA and cell membrane damage) will destroy them more efficiently [7, 14, 31]. According to the results, the minimum efficiency of DFW and HT-29 cell lines at radiation dose of 4 Gy and nanocomplex concentration of 4 mg/ml estimated to 13.22% and 21.23%, respectively. In addition, in accordance with the experimental studies [7], we simply called and estimated RT induced cell death as apoptotic death and PDT induced cell death as necrotic death during XPDT.

Treatment results showed that XPDT had the greatest effects on cell death due to the simultaneous effects of RT and PDT components. The estimated apoptotic and necrotic death of the cells during XPDT (4 Gy & 4 mg/ml) decreased cell population from 70% in RT (4 Gy) to about 30% for DFW cell line and from 65% in RT (4 Gy) to about 13% for HT29. As a result, XPDT has the potential to be used for radiation-resistant cell lines (like DFW) due to the presence of the PDT component and the potential to be used for deep-seated tumors (like HT29) due to the well penetration depth of 6 MV radiation. Moreover, results showed that XPDT was able to reduce cell viability more effective than RT in similar and low radiation doses, and also RT in the presence of radiosensitizers (RT+RS). So, it can predict that unwanted side effects of RT decreased during XPDT.

Although model results well followed experimental data in most of the conditions, but there were some special conditions that were not considered in the current model such as biostimulation of the cells due to production of light by scintillator or photoelectric phenomena inside the cells. In addition, further experimental and mathematical efforts are recommended to evaluate the long-term effects of XPDT such as colony assay and its effects.

Conclusion

Mathematical modeling of XPDT with emphasizing on the contribution of RT and PDT components, enables us to have a better estimation for treatment efficiency and makes it possible to understand the mechanism of this treatment more clearly. Although both experimental and mathematical results showed more XPDT efficiency in targeting cancer cells in comparison with RT and PDT alone, more studies are required to explain unpredicted cellular behavior at specific treatment conditions. Moreover, modeling of local oxygen effects make it possible to predict treatment results at different physiological conditions and explain the reason of low treatment efficiency in hypoxic tumor cells [41].

References

1. Shabanzadeh M, Mohammadi Z, Imanparast A, Sazgarnia A. Photosensitivity and Radiosensitivity of Methylene Blue (MB) With Gold Nanoparticles Coated By Thioglucose (Gnps-Tio): An In Vitro Study. Iranian Journal of Medical Physics/Majallah-I Fīzīk-I Pizishkī-i Īrān. 2023;20(3).
2. Borhani S, Mozdarani H, Babalui S, Bakhshandeh M, Nosrati H. In vitro radiosensitizing effects of temozolomide on U87MG cell lines of human glioblastoma multiforme. Iranian journal of medical sciences. 2017;42(3):258.
3. Hendee WR, Ibbott GS, Hendee EG. Radiation therapy physics: John Wiley & Sons; 2013.
4. Juzenas P, Chen W, Sun Y-P, Coelho MAN, Generalov R, Generalova N, et al. Quantum dots and nanoparticles for photodynamic and radiation therapies of cancer. Advanced drug delivery reviews. 2008;60(15):1600-14.
5. Wen X, Li Y, Hamblin MR. Photodynamic therapy in dermatology beyond non-melanoma cancer: An update. Photodiagnosis and photodynamic therapy. 2017;19:140-52.
6. Dolmans DE, Fukumura D, Jain RK. Photodynamic therapy for cancer. Nature reviews cancer. 2003;3(5):380-7.
7. Pass HI. Photodynamic therapy in oncology: mechanisms and clinical use. JNCI: Journal of the National Cancer Institute. 1993;85(6):443-56.
8. Tang R, Habimana-Griffin LM, Lane DD, Egbulefu C, Achilefu S. Nanophotosensitive drugs for light-based cancer therapy: what does the future hold? : Future Medicine. 2017;1101-5.
9. Wang GD, Nguyen HT, Chen H, Cox PB, Wang L, Nagata K, et al. X-ray induced photodynamic therapy: a combination of radiotherapy and photodynamic therapy. Theranostics. 2016;6(13):2295.
10. Sun W, Zhou Z, Pratx G, Chen X, Chen H. Nanoscintillator-mediated X-ray induced photodynamic therapy for deep-seated tumors: from concept to biomedical applications. Theranostics. 2020;10(3):1296.
11. Chen W, Zhang J. Using nanoparticles to enable simultaneous radiation and photodynamic therapies for cancer treatment. Journal of nanoscience and nanotechnology. 2006;6(4):1159-66.
12. Hosseini FS, Naghavi N, Sazgarnia A, and Vejdani Noghreiyan A. Modeling synergy and individual

effects of X-ray induced photodynamic therapy components. Scientific Reports. 2025;15(1): 453-467.
13. Morgan NY, Kramer-Marek G, Smith PD, Camphausen K, Capala J. Nanoscintillator conjugates as photodynamic therapy-based radiosensitizers: calculation of required physical parameters. Radiation research. 2009;171(2):236-44.
14. Bulin A-L, Vasil'Ev A, Belsky A, Amans D, Ledoux G, Dujardin C. Modelling energy deposition in nanoscintillators to predict the efficiency of the X-ray-induced photodynamic effect. Nanoscale. 2015;7(13):5744-51.
15. Klein JS, Sun C, Pratx G. Radioluminescence in biomedicine: physics, applications, and models. Physics in Medicine & Biology. 2019;64(4):04TR1.
16. Hosseini FS, Naghavi N, Sazgarnia A. A physicochemical model of X-ray induced photodynamic therapy (X-PDT) with an emphasis on tissue oxygen concentration and oxygenation. Scientific Reports. 2023;13(1): 17882-897.
17. Schwarz SB, Schaffer PM, Kulka U, Ertl-Wagner B, Hell R, Schaffer M. The effect of radio-adaptive doses on HT29 and GM637 cells. Radiation Oncology. 2008;3(1):1-6.
18. Khan MK, Khan N, Almasan A, Macklis R. Future of radiation therapy for malignant melanoma in an era of newer, more effective biological agents. OncoTargets and therapy. 2011:137-48.
19. Anderson AR. A hybrid mathematical model of solid tumour invasion: the importance of cell adhesion. Mathematical medicine and biology: a journal of the IMA. 2005;22(2):163-86.
20. Naghavi N, Hosseini FS, Sardarabadi M, Kalani H. Simulation of tumor induced angiogenesis using an analytical adaptive modeling including dynamic sprouting and blood flow modeling. Microvascular research. 2016;107:51-64.
21. Hosseini F, Naghavi N. Modelling tumor-induced angiogenesis: combination of stochastic sprout spacing and sprout progression. Journal of Biomedical Physics & Engineering. 2017;7(3):233.
22. Roghani Yazdi M, Naghavi N, Hosseini FS. Modeling and simulation of vascular tumor growth. Iranian Journal of Biomedical Engineering. 2015;9(2):143-61.
23. Yazdi MR, Naghavi N, Hosseini F. Numerical simulation of solid tumor invasion and metastasis with a continuum-discrete model. 2015 International Congress on Technology, Communication and Knowledge (ICTCK); 2015: IEEE.
24. Hosseini F, Naghavi N. Two dimensional mathematical model of tumor angiogenesis: coupling of avascular growth and vascularization. Iranian Journal of Medical Physics. 2015;12(3):145-66.
25. Shamsi M, Saghafian M, Dejam M, Sanati-Nezhad A. Mathematical modeling of the function of Warburg effect in tumor microenvironment. Scientific reports. 2018;8(1):8903.
26. Robertson-Tessi M, Gillies RJ, Gatenby RA, Anderson AR. Impact of metabolic heterogeneity on tumor growth, invasion, and treatment outcomes. Cancer research. 2015;75(8):1567-79.
27. Jalalimanesh A, Haghighi HS, Ahmadi A, Hejazian H, Soltani M. Multi-objective optimization of radiotherapy: distributed Q-learning and agent-based simulation. Journal of Experimental & Theoretical artificial intelligence. 2017;29(5):1071-86.
28. Shamsi M, Saghafian M, Dejam M, Sanati-Nezhad A. Mathematical modeling of the function of Warburg effect in tumor microenvironment. Scientific reports. 2018;8(1):1-13.
29. Noghreiyan AV. Photodynamic activation of silica / TiO2 / PpIX nanostructure by X-rays and its evaluation on survival of the human melanoma and colon cell lines: Mashad University of Medical Sciences, School of Medicine. 2020.
30. Goldman D, Popel AS. A computational study of the effect of capillary network anastomoses and tortuosity on oxygen transport. Journal of theoretical biology. 2000;206(2):181-94.
31. Ibrahim-Hashim A, Robertson-Tessi M, Enriquez-Navas PM, Damaghi M, Balagurunathan Y, Wojtkowiak JW, et al. Defining cancer subpopulations by adaptive strategies rather than molecular properties provides novel insights into intratumoral evolution. Cancer research. 2017;77(9):2242-54.
32. Molter TW, Holl MR, Dragavon JM, McQuaide SC, Anderson JB, Young AC, et al. A new approach for measuring single-cell oxygen consumption rates. IEEE transactions on automation science and engineering. 2008;5(1):32-42.
33. Gatenby RA, Gawlinski ET. The glycolytic phenotype in carcinogenesis and tumor invasion: insights through mathematical models. Cancer research. 2003;63(14):3847-54.
34. Patel AA, Gawlinski ET, Lemieux SK, Gatenby RA. A cellular automaton model of early tumor growth and invasion: the effects of native tissue vascularity and increased anaerobic tumor metabolism. Journal of theoretical biology. 2001;213(3):315-31.
35. Sazgarnia A, Bahreyni-Toosi MH, Montazerabadi AR, Ahmadi A. Indocyanine green acts as a photosensitizer but not a radiosensitizer: combined chemo-, photo-and radiotherapy of DFW human melanoma cells. Journal of Experimental Therapeutics and Oncology. 2013;10:189-96.
36. Yadollahpour A, Rezaee Z, Bayati V, Birgani MJT, Dehbashi FN. Radiotherapy enhancement with electroporation in human intestinal colon cancer HT-29 Cells. Asian Pacific journal of cancer prevention: APJCP. 2018;19(5):1259.
37. Georgakoudi I, Nichols MG, Foster TH. The mechanism of Photofrin photobleaching and its consequences for photodynamic dosimetry. Photochemistry and photobiology. 1997;65(1):135-44.
38. Hosseini FS, Naghavi N, Sazgarnia A. A physicochemical model of X-ray induced photodynamic therapy (X-PDT) with an emphasis on tissue oxygen concentration and oxygenation. Scientific Reports. 2023;13(1):17882.
39. Rezaei-Tavirani M, Dolat E, Hasanzadeh H, Seyyedi S-S, Semnani V, Sobhi S. TiO2 nanoparticle as a sensitizer drug in radiotherapy: in vitro study. International Journal of Cancer Management. 2013;6(Supplement).
40. Pan W, Gong S, Wang J, Yu L, Chen Y, Li N, et al. A nuclear-targeted titanium dioxide radiosensitizer for cell cycle regulation and enhanced radiotherapy. Chemical Communications. 2019;55(56):8182-5.

41. Noghreiyan AV, Soleymanifard S, Sazgarnia A. Design of a novel nanoparticle to use X-Ray fluorescence of TiO2 to induce photodynamic effects in the presence of PpIX. Photodiagnosis and Photodynamic Therapy. 2023:103890.